Electronic Supplementary Information

Biocompatible cracked reduced graphene oxide strain sensors: Enhancing implantable strain sensing performance and durability

Hyun Joo Lee[a, †], Bokyeong Ryu[b, †], Dong Keon Lee[c], Hyung Ju Park[d], Chul Huh[d], Dong Ick Son[e], Dong Han Ha[f], C-Yoon Kim[g,*], Yongseok Jun[a,h,*], and Yong Ju Yun[a,*]

[a]Department of Integrative Energy Engineering, & Graduate School of Energy and Environment (KU-KIST Green School), College of Engineering, Korea University, Seoul 02841, Republic of Korea. yjyun0@korea.ac.kr

[b]Department of Biomedical Informatics, College of Applied Life Sciences, Jeju National University, Jeju 63243, Republic of Korea

[c]Department of Emergency Medicine, Seoul National University Bundang Hospital, 82, Gumi-ro, Bundang-gu, Seongnam-si, Gyeonggi-do 13620, Republic of Korea.

[d]Electronics and Telecommunications Research Institute (ETRI), 218 Gajeong-ro, Yuseong-gu, Daejeon 34129, Republic of Korea

[e]Institute of Advanced Composite Materials, Korea Institute of Science and Technology, 92, Chudong-ro, Bongdong-eup, Wanju, Jeollabuk-do, 55324, Republic of Korea

[f]Interdisciplinary Materials Measurement Institute, Korea Research Institute of Standards and Science, 267, Gajeong-ro, Yuseong-gu, Daejeon 34113, Republic of Korea

[g]College of Veterinary Medicine, Konkuk University, 120 Neungdong-ro, Gwangjin-gu, Seoul 05029, Republic of Korea. E-mail: vivavet@konkuk.ac.kr

[h]Energy Materials Research Center, Clean Energy Research Division, Korea Institute of Science and Technology (KIST), Seoul 02792, Republic of Korea. yongseok@korea.ac.kr

Supplementary Methods and Discussion

1. Materials

Graphite powder (< 20 μm, 282863), hydroiodic acid (HI, 210021), 3-Aminopropyl triethoxysilane ($H_2N(CH_2)_3Si(OC_2H_5)_3$, 440140), sodium acetate ($NaC_2H_3O_2$, 241245), sodium bicarbonate ($NaHCO_3$, S8875), sulfuric acid (H_2SO_4, 258105), sodium nitrate ($NaNO_3$, 221341), and potassium permanganate ($KMnO_4$, 223468) were purchased from Sigma-Aldrich (Republic of Korea). Medical glue (n-Butyl-cyanoacrylate) was purchased from B. Braun (Republic of Korea). Sylgard 184 silicone elastomer kit was purchased from Dow Corning (Republic of Korea). All ultra-high purity nitrogen gas was purchased from Dongwon Gas (Republic of Korea).

2. Synthesis of GO flake

The GO flakes were synthesized from purified natural graphite by using the modified Hummers method. Typically, 1.5 g graphite powder was immersed into cold concentrated H_2SO_4 under ice bath. Then 1.0 g $NaNO_3$ and 6.0 g $KMnO_4$ was slowly added. All mixtures were kept at 40 °C for 2 hours for magnetic stirring. Then deionized water was added and kept the reation for 30 min. After 3 days, 10 ml 35% H_2O_2 was added until the color of the mixture changed to bright yellow. In order to remove metal ions, 100 ml HCl was added. The mixture was cleaned via high speed centrifugation (10,000 rpm). Deionized (DI) water was used to wash it via high speed centrifugation until pH = 7.0. Then collect the brown mixture in a clean beaker and add some more deionized water. Most of the as-synthesized GO flakes had a thickness of approximately 1.0 ± 0.2 nm with an average lateral size of 1.5 ± 1.0 μm, indicating the single-layer structure (Figure S4, Supporting Information). Subsequently, the colloidal dispersion of individual GO nanoflake in DI water at a concentration of 1.0 mg/ml was prepared using an high-power ultrasonic homogenizer (Sonoplus HD 2200, Bandelin Co.) with standard titanium tip in a 100 ml vessel for 30 min (Figure S4, Supporting Information).

3. Characterization

The surface morphology and detailed structure of the graphene strain sensors was analyzed using a field emission scanning electron microscope (FESEM, JEOL-6701F, JEOL Company, USA) and atomic force microsocpe (AFM, Veeco, Digital Instruments Dimension 3100 AFM with super sharp SSS-NCHR cantilever). Raman spectra were taken using Raman microscope system (inVia confocal Raman microscope, Renishaw plc, UK) with excitation energy of 2.41 eV, 514 nm laser to investigate the its quality. The contact angle was obtained by using a contact angle analyzer (DSA100, KRUSS GmbH) with physiological saline solution and DI water.

4. Culture of L929 fibroblasts with soft graphene films and strain sensors

To analyze cell morphological changes and viability, L929 fibroblasts (American Type Culture Collection® CCL-1™ NCTC clone 929) were chosen as recommended in ISO 10993-5 (ISO 2009). The cells were seeded at a density of 1.0 x 10^4 cells per well respectively of a 96-well culture plate (Eppendorf, Hamburg, Germany). The cells were subsequently cultured in RPMI 1640 media (Gibco, Grand Island, NY, USA) supplemented of 10% fetal bovine serum (FBS; Gibco, Grand Island, NY, USA) and 1X Antibiotic-Antimycotic (Gibco, Grand Island, NY, USA) in a humidified chamber under conditions of 37℃ and 5% CO_2. After 24 h of stabilization, the cells with 80% confluency were exposed to MWRGOcPDMS and MWRGOcPDMS sensors with gold electrode, negative control RM-C (high density polyethylene film; Food and Drug Safety Center (FDSC), Kanagawa, Japan), and positive control RM-B (polyurethane film containing 0.25% zinc dibuthyldithiocarbamate (ZDBC); FDSC, Kanagawa, Japan) with a tenth of culture area and incubated for 24 h. The control cells were maintained under untreated conditions to preserve the typical morphological characterizatics of fibroblasts. Additionally, the negative control group was intended to undergo the same incidental interventions including physical pressure by loaded RM-C, while the

positive control group underwent in vitro cellular toxicity of RM-B.

Subsequently, the morphological features of the cells were monitored using a microscope Eclipse TS100 (Nikon, Tokyo, Japan) and a software NIS-Elements Basic Research 3.22.00 (Nikon, Tokyo, Japan) (Figure 2a and Figure S12, Supporting Information).

5. MTT analysis for cell viability quantification

The cell viabilities were measured based on MTT assay as previously described at 24 h after sample treatment. Briefly, 3-(4,5-dimethylthiazol-2-yl)-2,5-diphenyltetrazolium bromide (MTT; Sigma-Aldrich, St Louis, MO, USA) was dissolved in phosphate-buffered saline (PBS; Gibco, Grand Island, NY, USA) at a concentration of 0.5 mg/ml. The culture media and samples were carefully and completely removed to prevent unnecessary physical trauma to the cells. The cells were subsequently incubated with 200 µl of 0.5 mg/ml MTT solution within the humidified incubating chamber (37°C) for 4 h to transform from MTT to 5-(4,5-dimethylthiazol-2-yl)-1,3-diphenylformazan (formazan). After 4 h of incubation, a half of the MTT solution was removed and 100 µl of dimethyl sulfoxide (DMSO; Sigma-Aldrich, St Louis, MO, USA) was added to each well. With DMSO, the plate was then gently agitated until the formazan crystal completely dissolved and the resulting solutions were aliquoted into a new 96-well plate. Absorbance of the aliquots was recorded at 570 nm using an Epoch Microplate Spectrophotometer (Bio-Tek Instruments Inc., Winooski, VT, USA). The viability of untreated cells was calculated as 100% alive. All experiments were performed in triplicate.

6. *In vivo* biosafety tests with MWRGOcPDMS graphene strain sensors

All of the animal experiments were carried out under the guidelines for the care and use of animals approved by Institutional Animal Care and Use Committee (IACUC) of Konkuk University (permission number: KU22162). For the experiments, thirty male BALB/c mice aged 6 weeks were chosen as recommended in ISO 10993-2 (ISO 2006). The mice were obtained (Jabio, Suwon, Korea) and housed in cages for a week to acclimatize the experimental conditions with an artificial 12:12 light/dark cycle, 22 ± 1°C of temperature, and 55 ± 10% of humidity. After acclimatization body weighted ~21.5 g, the mice were randomly divided into six groups. When aged 7 weeks with body weight ~21.5 g, the mice were randomly divided into six groups including (i) control (untreated), (ii) negative control, (iii) positive control, (iv) MWRGOcPDMS, (v) MWRGOcPDMS (gold toward muscle), and (vi) MWRGOcPDMS (gold toward skin). While the untreated control group was designed to represent normal physiologic al and histopathological conditions, the negative and positive control groups were designed to indicate that all experiments were conducted properly. The negative control group, which was equivalent to the sham control, was designed to undergo the same surgical and procedural inte rventions as the groups (iv), (v), and (vi) with the sample insertion except that this group recie ved a non-toxic RM-C (FDSC, Kanagawa, Japan) subcutaneously to mimic any incidental eff ects caused by the operation. Additionally, to ensure that all experiments were conducted corr ectly, the positive control group was designed to undergo the subcutaneous insertion of RM-B (FDSC, Kanagawa, Japan), a substance known to exhibit toxicity in both in vivo and in vitro. The implantation surgery was conducted according to ISO 10993-6 (ISO 2007). All the mice were anesthetized using 5% isoflurane for induction and 2% for maintenance. The mouse back hairs were subsequently shaved, and the underlying skin was cleaned using 70% ethyl alcohol. Throughout the surgical procedures, all strict sterility measures were upheld for survival surgeries. With appropriate depth of anesthesia, incisions were made on the dorsal section of

each mouse to implant samples with ~10.0 mm of width. MWRGOcPDMS sensor, MWRGOcPDMS with gold electrode, negative control RM-C (FDSC, Kanagawa, Japan), and positive control RM-B (FDSC, Kanagawa, Japan) were separately and independently implanted subcutaneously into each mouse. The MWRGOcPDMS strain sensors with gold electrode were implanted to Au face the muscle or the skin. The incisions were sutured using 6-0 nylon suture and povidone-iodine was topically applied to the surgery sites. All the mice were clinically monitored every day and the body weights were recorded for 2 weeks (Figure S13, Supporting Information). At 2 weeks after the implantation, all the mice were sacrificed using a CO_2 chamber and the gross lesions of subcutaneous regions were evaluated. Full-thickness skins were excised for histopathological analysis.

7. Histopathological analysis of mouse skin samples

To analyze the histopathological changes, the freshly excised skin samples were fixed with 4% neutralized phosphate-buffered formalin for 24 h. Subsequently, the tissues were processed by routine tissue techniques using a Tissue-Tek® VIP™ 5 Jr Tissue Processor (SAKURA, Staufen, Germany) and embedded in paraffin using a HistoCore Arcadia (Leica, Wetzlar, Germany). The paraffin-embedded specimens were cut into 4-μm-thick sections. The sections were mounted on slides (Marienfeld, Lauda-Königshofen, Germany) and stained with hematoxylin and eosin (H&E). Stained slides were evaluated using a camera TI-E 5.01 (Nikon, Tokyo, Japan) and a software NIS-Elements Advanced Research 4.13.01 (Nikon, Tokyo, Japan) to assess general histological changes. Histological lesions were monitored including mononuclear cell infiltration and thickening of the hypodermis (Figure S14, Supporting Information).

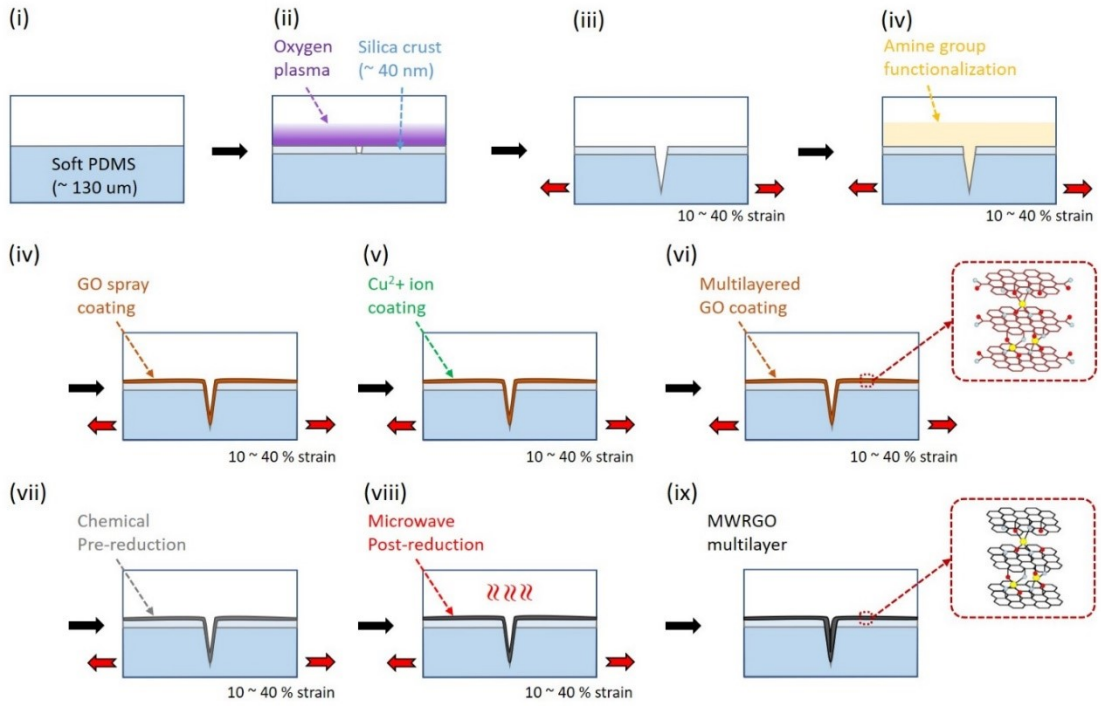

Figure S1. Process used for fabricating cracked RGO strain sensors.

Sample	Oxygen plasma treated PDMS film		
	1	2	3
AFM	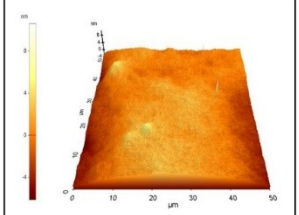	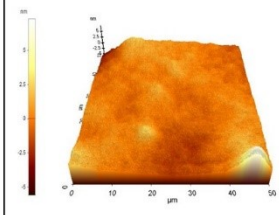	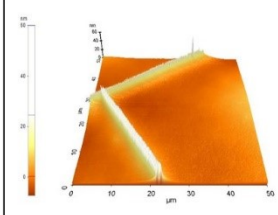
Detailed surface topology of Sample 3	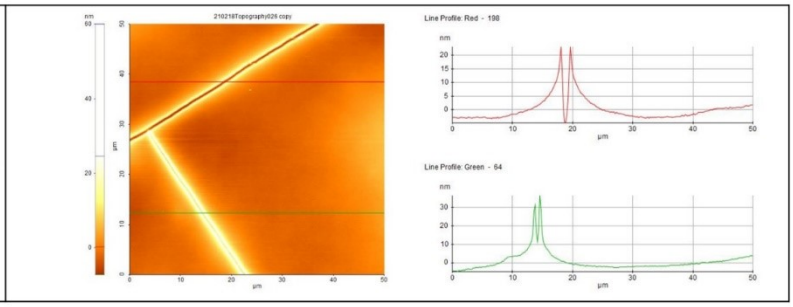		

Sample	Oxygen Plasma treatment			Surface topology of oxygen plasma treated PDMS		
	Chamber pressure (mTorr)	RF power (W)	Exposure time (s)	Crack formation	Crack depth (nm)	Crack width (nm)
1	300	12	60	X	-	-
2	300	12	120	X	-	-
3	300	12	300	O	40 ± 5	80 ± 30

Figure S2. Preparation and characterization of oxygen plasma treated PDMS films

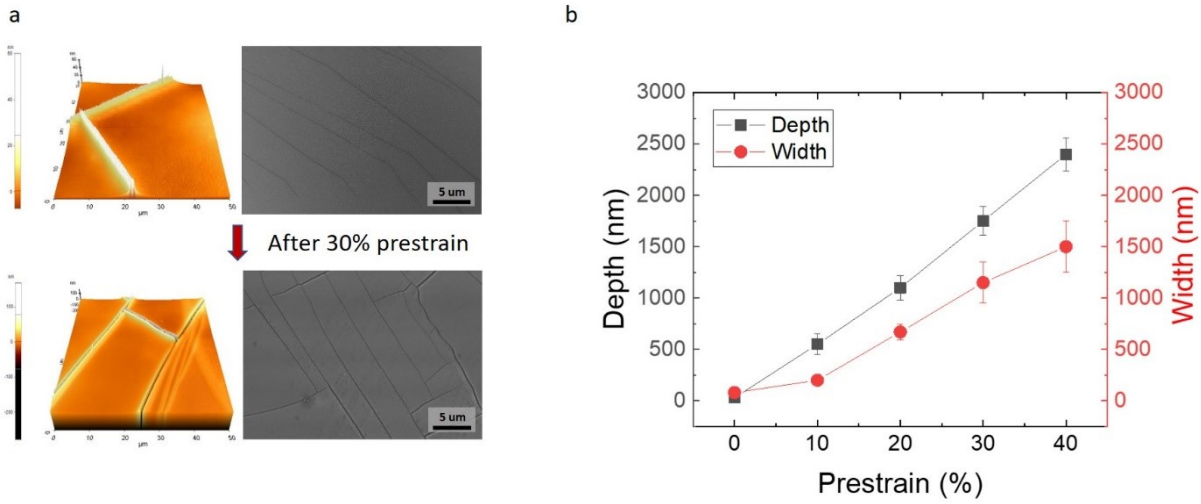

Figure S3. Surface topology of cPDMS substrate with various prestrain levels.
a, AFM and FESEM images of cPDMS after 40% prestrain at 100 cycles. b, Average depth and width of micro-cracks under different prestrains (10 to 40%).

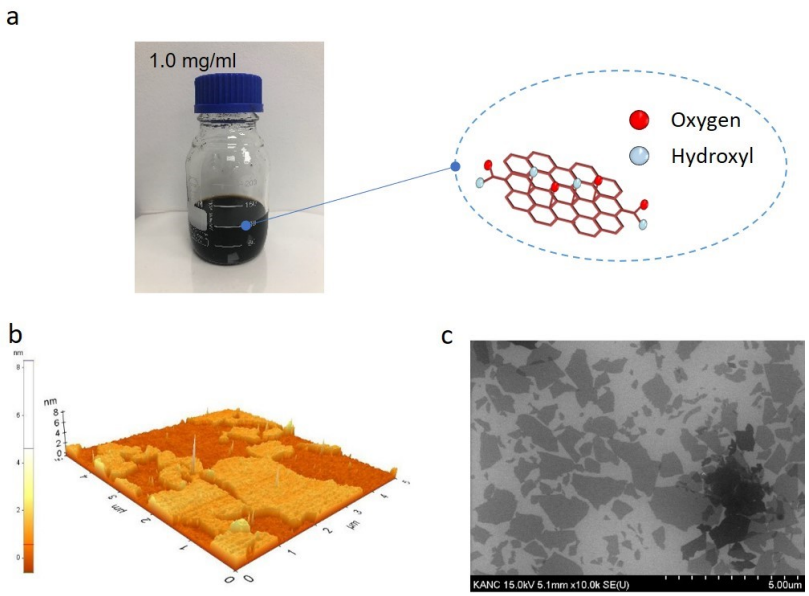

Figure S4. Characterization of GO flakes. a, Photograph of GO solution (1.0 mg/ml). b, c, FESEM image and 3D tapping mode AFM image profile of GO flakes on silicon substrates.

a, Photograph of reduction process of GOcPDMS film

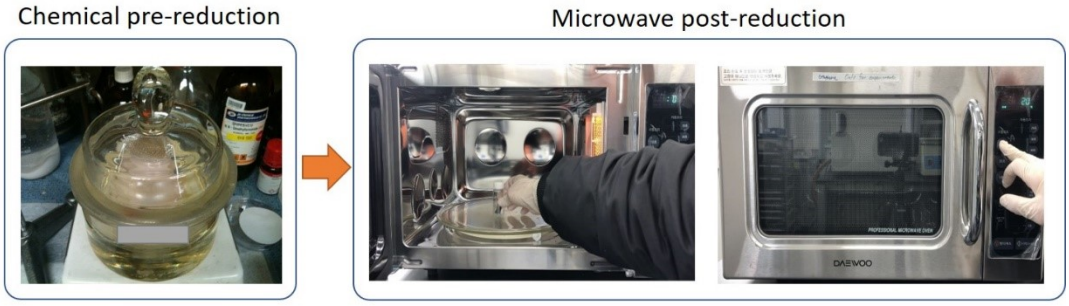

b, Detailed information of reduction process

RGOcPDMS film	Chemical pre-reduction with HI	Microwave post-reduction	Remark
CR0	X	X	
CR1	1 min	X	
CR2	2 min	X	
CR5	5 min	X	
CR10	10 min	X	
CR10+MR1	10 min	10 sec	20 W Ar gas
CR10+MR2	10 min	20 sec	20 W Ar gas

Figure S5. Hybrid reduction process of MGOcPDMS films

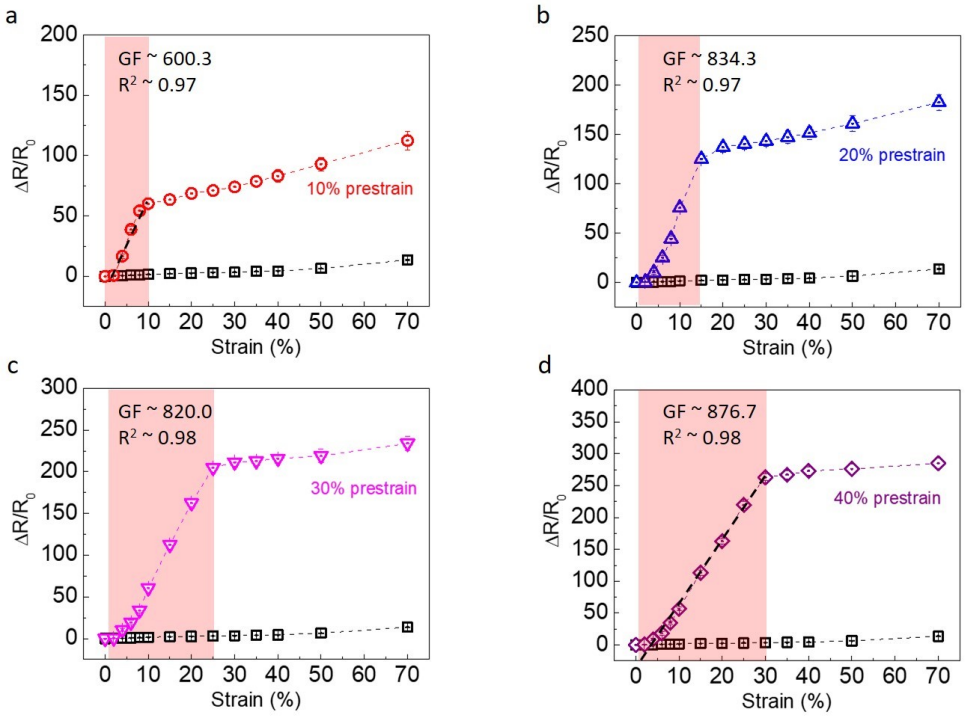

Figure S6. Strain sensing performance of the MWRGOcPDMS graphene strain sensors produced with different prestrain levels. (a) 10% prestrain (b) 20% prestrain (c) 30% prestrain (d) 40% prestrain.

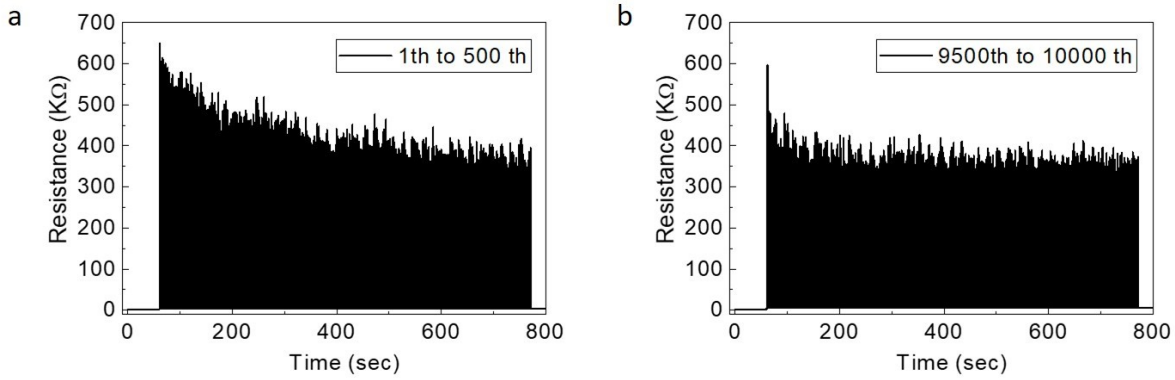

Figure S7. Long-term stability of the MWRGOcPDMS strain sensor produced with 20% prestrain level.

a

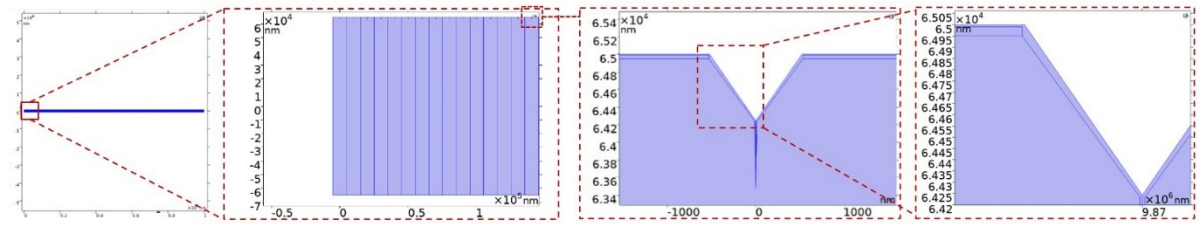

b

	MWRGO layer	Oxidized PDMS layer	PDMS substrate
Configuration	Top layer	Middle layer	Bottom layer
Dimension (Thickness)	~ 10 nm	~ 40 nm [6]	130 um
Density [kg/m^3]	2267 [1]	2200 [7]	965 [8]
Electrical conductivity [S/cm]	1.19 x 10^2	1.5 x 10^{-11} [7]	2.5 x 10^{-16} [8]
Thermal conductivity [W/(m K)]	1000 ~ 5000 [2]	0.6 [7]	0.15 [8]
Dielectric constant	3.4~5.8 [3]	3.6 [7]	2.6 [9]
Young's modulus [GPa]	250 [4]	1.5 [6]	1.1 x 10^{-3} [10]
Poisson ratio	0.2 [5]	0.17 [7]	0.499 [9]
Contact angle [degree]	~ 110	~ 5 [6]	113.5 [8]

Figure S8. a,b, The structures and parameters of the MWRGOcPDMS strain sensor for FEA simulation.

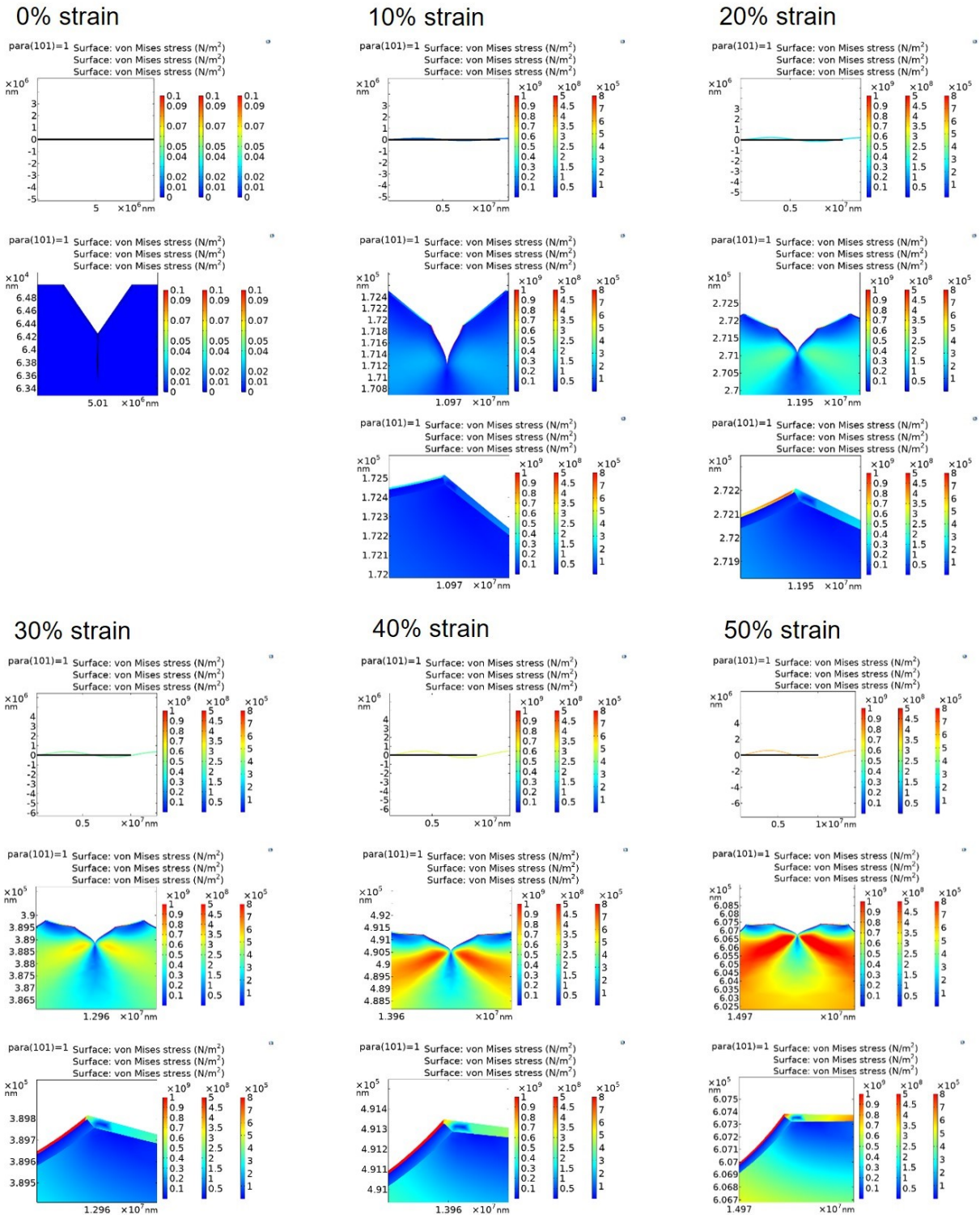

Figure S9. Simulation results of stress distribution of the MWRGOcPDMS strain sensor with 40% prestrain under 0, 10, 20, 30, 40, 50 % strain

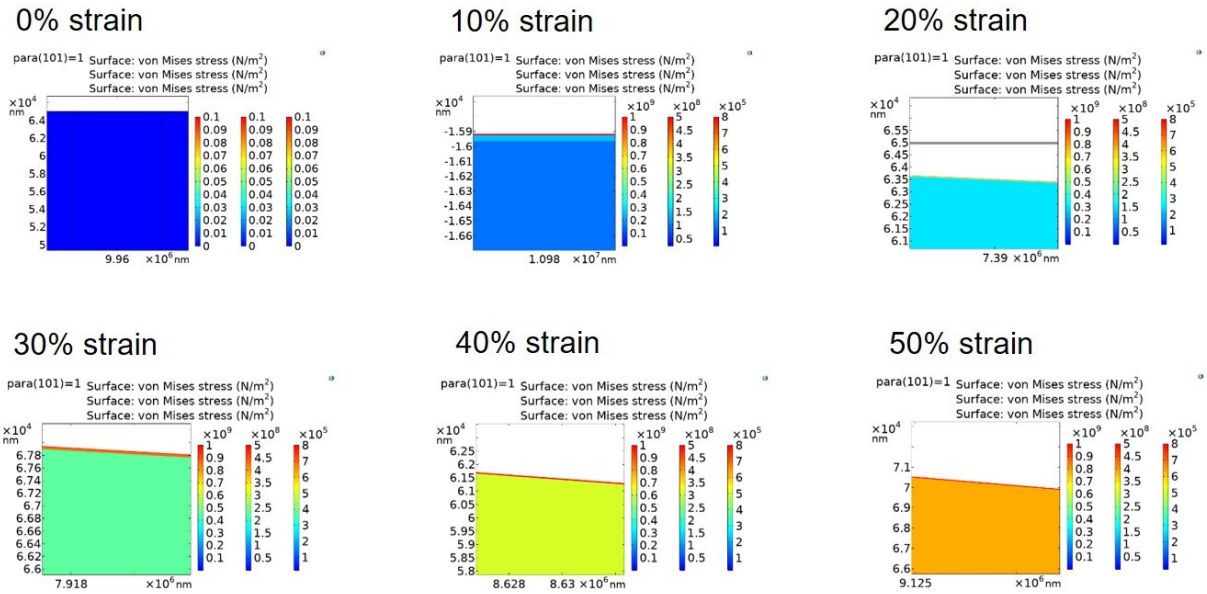

Figure S10. Simulation results of the MWRGOPDMS film without microcrack pattern under 0, 10, 20, 30, 40, 50 % strain

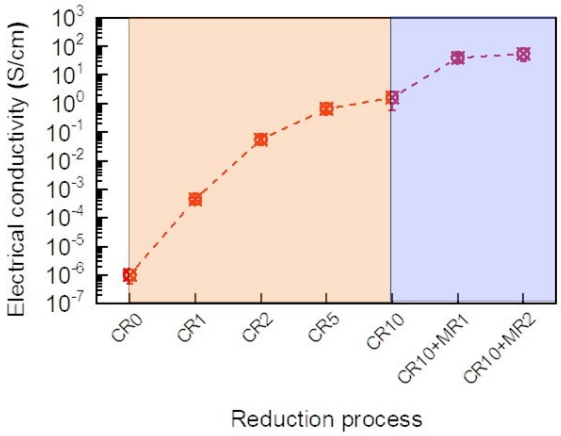

Figure S11. Variation of electrical conductivity of the MWRGOcPDMS films dependent on hybrid reduction process.

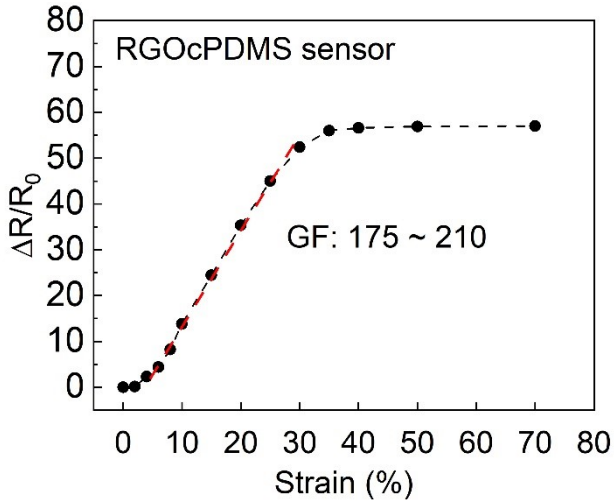

Figure. S12. Sensor performance of RGOcPDMS graphene strain sensors with 40% prestrained substrate.

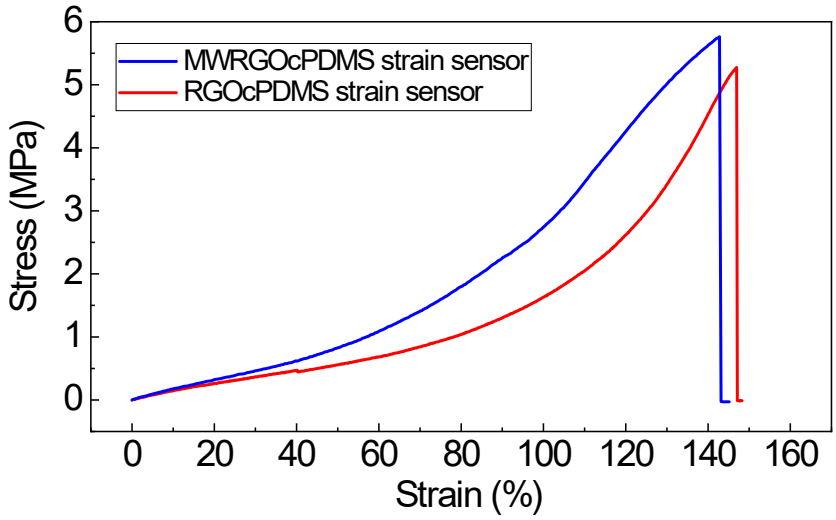

Figure S13. Stress-strain curves for RGOcPDMS and MWRGOcPDMS strain sensors.

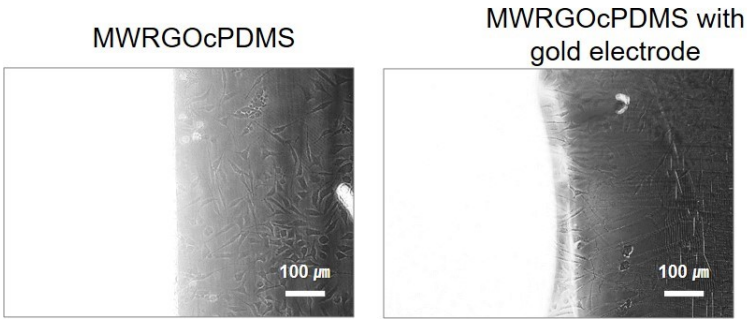

Figure S14. Microscopic images harvested with a stronger illumination. L929 fibroblasts were exposed with the MWRGOcPDMS graphene sensors without gold electrode (left) and with gold electrode (right) for 24 h. The scale bars are 100 μm.

	Naïve control					Negative control					Positive control				
POD 0	20.66	21.11	21.51	21.90	22.22	20.83	21.00	21.45	22.00	22.35	20.55	21.50	21.58	22.08	22.22
POD 1	21.17	21.39	21.55	22.06	22.25	20.81	21.00	21.05	21.85	22.10	21.93	22.00	22.13	22.45	22.54
POD 2	21.10	21.38	21.58	21.96	22.26	20.94	21.18	21.23	21.90	22.15	21.75	21.81	21.98	22.12	22.26
POD 3	21.62	22.03	22.13	22.27	22.83	21.39	21.57	21.63	21.82	22.41	22.21	22.47	22.64	22.75	23.09
POD 4	21.74	22.00	22.15	22.63	23.02	21.67	21.87	21.95	22.44	22.84	22.19	22.36	22.49	22.88	23.10
POD 5	22.07	22.31	22.50	22.69	23.23	21.99	22.11	22.31	22.43	23.17	22.56	22.69	22.79	23.16	23.48
POD 6	22.38	22.63	22.72	23.30	23.78	22.39	22.55	22.66	22.98	23.52	22.63	22.90	22.99	23.63	23.93
POD 7	22.52	22.59	22.88	23.12	23.62	22.34	22.39	22.74	22.79	23.67	22.91	22.91	22.94	23.56	23.87
POD 8	22.41	22.53	22.86	23.13	23.47	22.42	22.52	22.69	23.00	23.22	22.82	23.06	23.27	23.39	23.82
POD 9	22.12	22.98	23.19	23.28	23.81	22.26	23.19	23.20	23.31	23.60	21.98	23.33	23.49	23.51	24.06
POD 10	22.39	22.71	23.00	23.19	23.66	22.51	22.70	22.80	23.03	23.50	22.93	23.17	23.48	23.55	23.84
POD 11	22.45	23.02	23.27	23.53	24.06	22.54	23.03	23.16	23.35	23.69	22.39	23.41	23.64	23.69	24.38
POD 12	22.38	22.90	23.13	23.25	23.84	22.59	22.87	22.90	23.06	23.77	23.03	23.27	23.69	23.70	23.85
POD 13	22.78	23.06	23.35	23.77	24.30	22.82	22.87	23.11	23.38	23.78	22.80	23.48	23.78	23.86	24.69
POD 14	22.42	22.69	23.05	23.12	23.86	22.80	22.83	23.25	23.26	23.84	22.82	22.97	23.54	23.59	24.50
	MWRGOcPDMS					Gold/MWRGOcPDMS toward mus					Gold/MWRGOcPDMS toward skin				
POD 0	20.76	20.98	21.65	21.78	22.24	20.68	21.58	21.13	21.68	21.56	20.81	21.43	21.79	21.80	21.41
POD 1	20.92	21.33	21.61	22.04	22.26	20.95	21.73	21.34	21.96	21.71	20.83	21.35	21.65	21.82	21.33
POD 2	20.77	21.29	21.69	22.02	22.53	21.00	21.70	21.35	22.02	21.68	20.87	21.56	21.81	21.87	21.54
POD 3	21.42	22.20	22.27	22.39	23.14	21.45	22.30	21.88	22.49	22.28	21.13	22.09	22.39	22.14	22.07
POD 4	21.53	21.94	22.18	22.73	23.29	21.70	22.40	22.05	22.75	22.38	21.70	22.19	22.35	22.73	22.17
POD 5	21.81	22.28	22.56	22.65	23.19	22.01	22.82	22.42	23.08	22.80	22.01	22.69	22.84	23.06	22.66
POD 6	22.02	22.33	22.41	23.17	23.79	22.39	23.10	22.75	23.48	23.08	22.52	22.82	22.88	23.60	22.80
POD 7	22.20	22.36	22.85	22.90	23.23	22.38	23.15	22.77	23.47	23.13	22.60	22.99	23.00	23.70	22.97
POD 8	22.13	22.15	22.77	23.14	23.53	22.04	23.32	22.68	23.11	23.30	22.57	22.61	23.06	23.65	22.59
POD 9	22.27	22.57	23.01	23.16	23.92	22.47	23.28	22.88	23.56	23.26	22.74	22.86	23.43	23.84	22.84
POD 10	21.90	22.43	22.86	23.14	23.79	22.31	23.46	22.88	23.39	23.44	22.70	22.76	23.09	23.79	22.73
POD 11	22.56	22.77	23.16	23.69	24.25	22.76	23.35	23.06	23.86	23.33	22.86	22.98	23.50	23.96	22.95
POD 12	21.66	22.70	22.95	23.13	24.04	22.57	23.60	23.09	23.66	23.58	22.83	22.90	23.12	23.92	22.88
POD 13	22.55	22.66	23.01	23.91	24.28	23.05	23.42	23.24	24.17	23.40	22.97	23.09	23.57	24.09	23.07
POD 14	22.41	23.04	23.13	23.26	24.00	22.67	23.07	22.87	23.77	23.05	22.77	23.37	23.63	23.86	23.35

Figure S15. Body weight of mice after implantation of the MWRGOcPDMS graphene sensor. BALB/c mice were implanted with samples subcutaneously for 2 weeks. Each of the body weights was monitored every single day after the implantation.

a

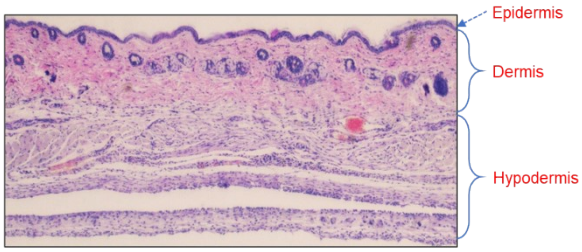

b

Hypodermis thickness (μ	Mouse 1			Mouse 2			Mouse 3			Mouse 4			Mouse 5		
	HPF 1	HPF 2	HPF 3	HPF 1	HPF 2	HPF 3	HPF 1	HPF 2	HPF 3	HPF 1	HPF 2	HPF 3	HPF 1	HPF 2	HPF 3
sham control	147.40	120.60	140.03	191.62	156.78	182.04	153.30	125.42	145.64	199.28	163.05	189.32	176.88	144.72	168.04
negative control	136.58	166.93	129.75	183.62	150.23	174.44	146.89	120.19	139.55	156.24	190.96	148.43	129.75	158.58	123.26
positive control	397.65	325.35	377.77	357.89	437.42	340.00	286.31	349.93	271.99	454.91	372.20	432.16	377.77	309.08	358.88
RGO	135.00	165.00	128.25	181.50	148.50	172.43	145.20	118.80	137.94	154.44	188.76	146.72	175.50	214.50	166.73
AuRGO_Au to muscle	136.13	111.38	129.32	155.93	190.58	148.13	124.74	152.46	118.50	198.20	162.16	188.29	149.74	122.51	142.25
AuRGO_Au to skin	211.50	258.50	200.93	206.80	169.20	196.46	165.44	135.36	157.17	175.97	215.07	167.17	148.05	180.95	140.65

Hypodermis thickness (μ	Mouse Avrg	Mouse Avrg	Mouse Avrg	Mouse Avrg	Mouse 5 Avrg
sham control	136.01	176.81	141.45	183.88	163.21
negative control	144.42	169.43	135.54	165.21	137.20
positive control	366.92	378.44	302.74	419.76	348.58
RGO	142.75	167.48	133.98	163.31	185.58
AuRGO_Au to muscle	125.61	164.88	131.90	182.88	138.17
AuRGO_Au to skin	223.64	190.82	152.66	186.07	156.55

Figure S16. The thickness of the hypodermis layer. a, A representative image of full-thickness skin is provided with labelings for microscopic structures. b, The hypodermis thickness was measured in three random high-power fields (HPFs) of each samples.

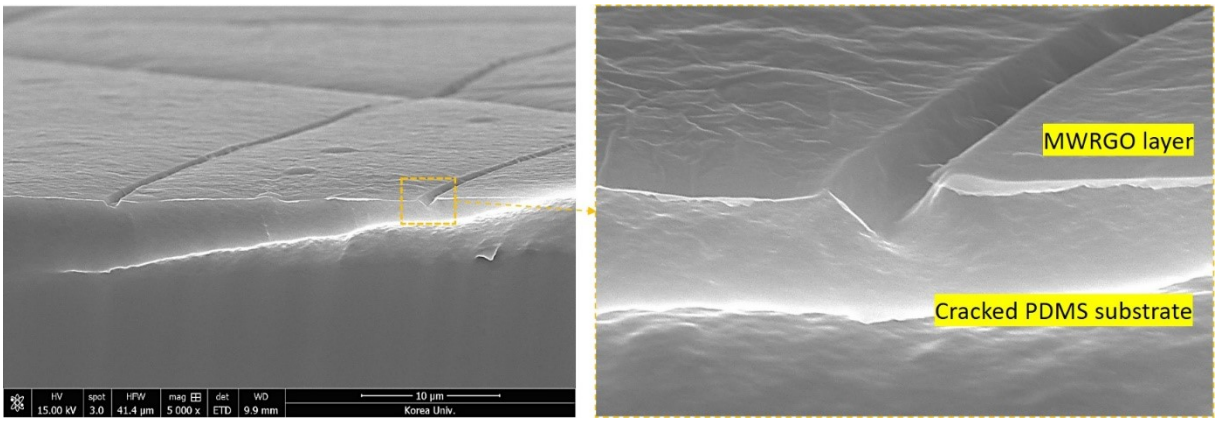

Figure S18. FESEM results of the MWRGOcPDMS strain sensor under 20% strain.

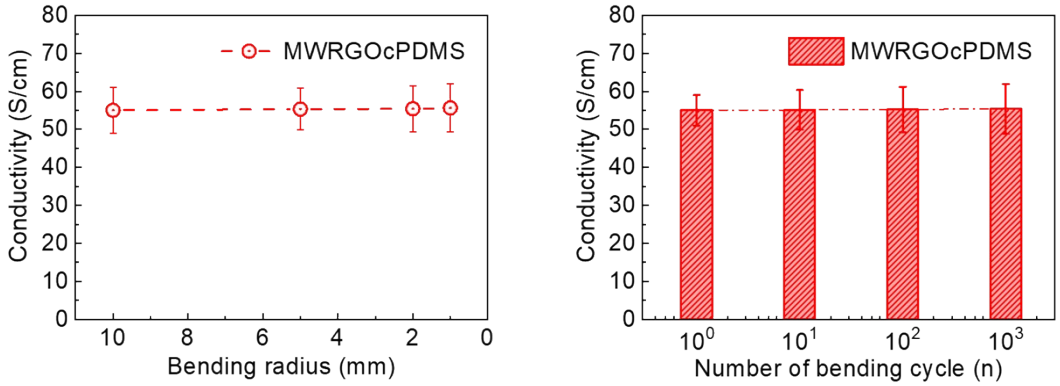

Figure S19. a, Variation in conductivity of the MWRGOcPDMS strain sensors as a function of bending radius. b, Variation in the conductivity ratio of the MWRGOcPDMS sensors as a function of the number of bending cycles for the radius of bending (2.0 mm). Figure S19 shows the variations in the electrical conductivities of the MWRGOcPDMS strain sensor, measured as a function of the bending radius from 10.0 to 1.0 mm. The sensor do not exhibit noticeable changes in the conductivity at a bending of 1.0 mm.

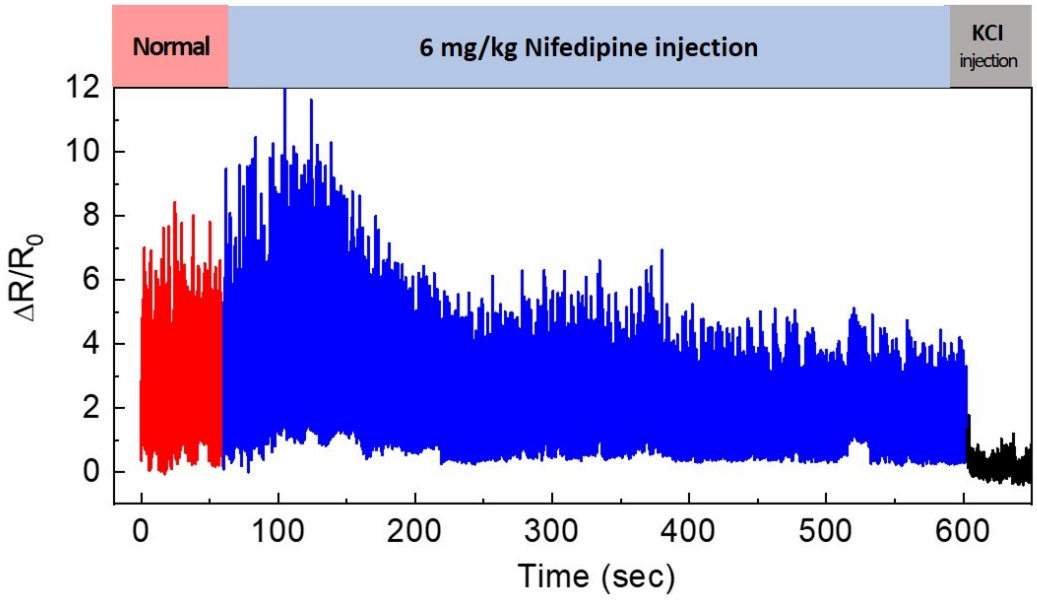

Figure S20. Representative traces of change in sensor resistance ratio when exposed to 6 mg/kg nifedipine IV injection and KCl IV injection.

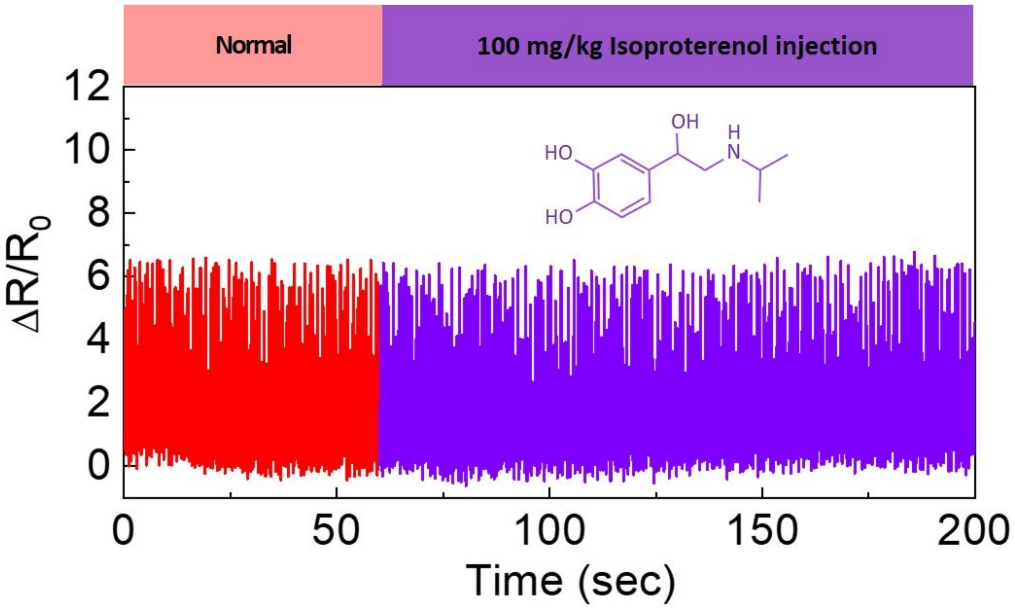

Figure S21. Representative traces of change in sensor resistance ratio when exposed to 100 mg/kg isoproterenol IV injection.

Table S1. Comparison of sensor performance with previously reported implantable strain sensors

Sensor material	Type	Gauge factor or sensitivity (GF)	Long-term Stability (Cycles)	Chemical stability in PBS solution	Biocompatibility		Animal model	Target tissue /organ	Ref
					In vitro Cell viability	In vivo			
Microwaved RGO/ cracked PDMS	Resistive	876.7	10,000	No Passivation	Excellent	Excellent	Rat	Heart	This work
Silicon membrane/ PI	Piezo resistive	-0.06~0.33	Not shown	Polyimide Passivation	Not Shown	Not shown	Rabbit	Heart	11
Mg/PLLA/ POMaC	Capacitive	Not shown	20,000	PoMac passivation	Excellent	Excellent	Rat	tendon	12
Au-TiO2 nanowire composite/ PDMS	Resistive	Not shown	100,000	PDMS passivation	Not Shown	Not shown	Pig	Heart	13
PEDOT:PSS /glycerol/VP	Resistive	Not shown	10,000	Visco PDMS Passivation	Excellent	Excellent	Rat	Leg	14
Liquid metal/ PAAm–alginate hydrogels	Resistive	Not shown	Not shown	Hydrogel Passivation	Good	Not shown	Rabbit	heart	15
Silicon membrane/ PI	Piezo resistive	1.5	3,000	Diluted PI Passivation	Excellent	Excellent	Rat	bladder	16
Ecoflex-carbon black blend/ ecoflex/ DST hydrogel	Resistive	Not shown	5,000	No Passivation	Excellent	Excellent	Pig	Heart	17

Table S2. Information on the physiological status of rats and the drug administrated.

Subject Number (#)	Animal model (sex, body weight)	Mechanical ventilator (breaths per minute)	Drug (dose)	Injection method (IP, IV)
5	Sprague Dawley rat (Female, 155 g)	Yes (81/min)	Nifedipine (30 mg/kg)	IV
6	Sprague Dawley rat (Male, 230 g)	Yes (79/min)	Nifedipine (30 mg/kg)	IP
7	Sprague Dawley rat (Male, 230 g)	Yes (79/min)	Nifedipine (6 mg/kg)	IV
8	Sprague Dawley rat (Male, 230 g)	Yes (79/min)	KCl (2 mmol/kg)	IV
9	Sprague Dawley rat (Male, 240 g)	Yes (78/min)	Isoproterenol (100 mg/kg)	IP
10	Sprague Dawley rat (Male, 180 g)	Yes (83/min)	Isoproterenol (100 mg/kg)	IV
11	Sprague Dawley rat (Male, 180 g)	Yes (83/min)	Nifedipine (30 mg/kg)	IV

Supplementary Video

Supplementary Video 1. Comparison of FEA simulation results of the MWRGOcPDMS strain sensor and MWRGOPDMS strain sensor without microcrack patterns.

Supplementary Video 2. Implantable graphene strain sensors that operated on rat heart for detecting cardiac contractility.

Supplementary References

1. M. J. Allen, V. C. Tung, R. B. Kaner, *Chem. Rev.,* **2010**, 110, 132.
2. A. A. Balandin, S. Ghosh, W. Bao, I. Calizo, D. Teweldebrhan, F. Miao, C. N. Lau, *Nano Lett.*, **2008**, 8, 902.
3. E. J. Santos, E. Kaxiras, *Nano Lett.,* **2013**, 13, 898.
4. Y. Zhu, S. Murali, W. Cai, X. Li, J. W. Suk, J. R. Potts, R. S. Ruoff. *Adv. Mater.,* **2010**, 22, 3906.
5. G. Cao, *Polymers*., **2014**, 6, 2404.
6. S. Befahy, P. Lipnik, T. Pardoen, C. Nascimento, B. Patris, P. Bertrand, S. Yunus, *Langmuir*, **2010**, 26, 3372.
7. J. F. Shackelford, Y.-H. Han, S. Kim, S.-H. Kwon, CRC materials science and engineering handbook - 4th ed, CRC Press, **2016**.
8. J. C. McDonald, G. M. Whitesides, *Acc. Chem. Res.,* **2002**, 35, 491.
9. J. E. Mark, Polymer data handbook, Oxford Univ. Press, New York, **1999**.
10. M. Liu, J. Sun, Y. Sun, C. Bock, Q. Chen, *J. Micromech. Microeng.,* **2009***,* 19, 035028.
11. L. Xu, S. R. Gutbrod, A. P. Bonifas, Y. Su, M. S. Sulkin, N. Lu, H.-J. Chung, K.-I Jang, Z. Liu, M. Ying, C. Lu, R. C. Webb, J.-S. Kim, J. I. Laughner, H. Cheng, Y. Liu, A. Ameen, J.-W. Jeong, G.-T. Kim, Y. Huang, I. R. Efimov, J. A. Rogers, *Nat. Commun.,* **2014***,* 5, 3329.
12. C. M. Boutry, Y. Kaizawa, B. C. Schroeder, A. Chortos, A. Legrand, Z. Wang, J. Chang, P. Fox, Z. Bao, *Nature Electronics,* **2018***,* 1, 314.
13. S. A. Dual, B. L. Zambrano, S. Sundermann, N. Cesarovic, M. Kron, K. Magkoutas, J. Hengsteler, V. Falk, C. Starck, M. Meboldt, J. Voros, M. S. Daners, *Adv Health Mater*, **2020**, 9, 2000855.
14. Y. Liu, J. Li, S. Song, J. Kang, Y. Tsao, S. Chen, V. Mottini, K. McConnell, W. Xu, Y.-Q. Zheng, J. B.-H. Tok, P. M. George, Z. Bao, *Nat. Biotech.* **2020**, 38, 1031.
15. Y. Liu, T. Yang, T. Zhang, G. Qu, S. Wei, Z. Liu, T. Kong, *Adv. Mater.* **2019**, 31, 1902783.
16. T. M. Jang, J. H. Lee, H. Zhou, J. Joo, B. H. Lim, H. Cheng, S. H. Kim, I.-S. Kang, K.-S. Lee, E. Park, S.-W. Hwang, *Sci. Adv.,* **2020**, 6:eabc9675.
17. H. Yuk, C. E. Varela, C. S. Nabzdyk, X. Mao, R. F. Padera, E. T. Roche, X. Zhao, *Nature,* 2019, 575, 169.